How to cite: *Angew. Chem. Int. Ed.* **2025**, *64*, e202416605
doi.org/10.1002/anie.202416605

Perovskite Solar Cells | Hot Paper

Simultaneous Suppression of Multilayer Ion Migration via Molecular Complexation Strategy toward High-Performance Regular Perovskite Solar Cells

Qian Zhou, Yingying Yang, Dongmei He, Ke Yang, Yue Yu, Xinxing Liu, Jiajia Zhang,* Xuxia Shai, Jinsong Wang, Jianhong Yi, Meicheng Li,* and Jiangzhao Chen**

Abstract: The migration and diffusion of Li^+, I^- and Ag impedes the realization of long-term operationally stable perovskite solar cells (PSCs). Herein, we report a multifunctional and universal molecular complexation strategy to simultaneously stabilize hole transport layer (HTL), perovskite layer and Ag electrode by the suppression of Li^+, I^- and Ag migration via directly incorporating bis(2,4,6-trichlorophenyl) oxalate (TCPO) into HTL. Meanwhile, TCPO co-doping results in enhanced hole mobility of HTL, advantageous energy band alignment and mitigated interfacial defects, thereby leading to facilitated hole extraction and minimized nonradiative recombination losses. TCPO-doped regular device achieves a peak power conversion efficiency (PCE) of 25.68 % (certified 25.59 %). The unencapsulated TCPO doped devices maintain over 90 % of their initial efficiencies after 730 h of continuous operation under one sun illumination, 2800 h of storage at 30 % relative humidity, and 1200 h of exposure to 65 °C, which represents one of the best stabilities reported for regular PSCs. This work provides a new approach to enhance the PCE and long-term stability of PSCs by host–guest complexation strategy via rational design of multifunctional ligand molecules.

Introduction

In the field of environment and energy, the intensification of global climate change has prompted policymakers in various countries to regard the development and application of renewable energy as a top priority.[1,2] Many countries have successively introduced policies to reduce carbon emissions, creating a good development environment for the advancement of solar energy technology.[3,4] As an efficient and clean energy, solar energy plays a key role in achieving these goals and has become an important factor in promoting sustainable development.[5] In particular, perovskite solar cells (PSCs) have attracted widespread attention from researchers in the past decade due to their unique optoelectronic properties, low-cost manufacturing processes and versatile application scenarios.[6–17] Although the power conversion efficiency (PCE) of PSCs in the laboratory has exceeded 26 %, they still face many limitations and challenges in practical applications.[18–21] On the one hand, the present state-of-the-art PCE still falls short of the theoretical Shockley–Queisser limit.[22] The effective strategy needs to be explored to minimize nonradiative recombination losses, aiming to further overcome the bottleneck of efficiency improvement. On the other hand, the poor long-term stability presents a serious challenge for the commercial deployment of perovskite photovoltaic technology.

Currently, the stability of n-i-p (also known as regular) PSCs is extensively demonstrated to be inferior to that of p-i-n (also known as inverted) PSCs, which is primarily due to the indispensable use of 2,2′,7,7′-tetrakis (N, N-di-p-methoxyaniline)-9,9′-spirobifluorene (Spiro-OMeTAD) hole

[*] D. He, Y. Yu, X. Liu, J. Wang, J. Yi, J. Chen
Faculty of Materials Science and Engineering, Kunming University of Science and Technology, 650093 Kunming, China
E-mail: dmhe@kust.edu.cn
jzchen@kust.edu.cn

Q. Zhou[+]
Key Laboratory of Optoelectronic Technology & Systems (Ministry of Education), College of Optoelectronic Engineering, Chongqing University, 400044 Chongqing, China

Y. Yang,[+] M. Li
State Key Laboratory of Alternate Electrical Power System with Renewable Energy Sources, School of New Energy, North China Electric Power University, 102206 Beijing, China
E-mail: mcli@ncepu.edu.cn

K. Yang
Chongqing Institute of Green and Intelligent Technology, Chinese Academy of Sciences, 400714 Chongqing, China

J. Zhang
Anhui Provincial Key Laboratory of Green Carbon Chemistry, College of Chemistry and Materials Engineering, Fuyang Normal University, 236037 Fuyang, China
E-mail: jjzh@wxc.edu.cn

X. Shai
Institute of Physical and Engineering Science/Faculty of Science, Kunming University of Science and Technology, 650500 Kunming, China

transport layer (HTL) doped with bis(trifluoromethane) sulfonimide lithium salt (Li-TFSI) and 4-tert-butylpyridine (*t*BP) in high-efficiency regular devices. These dopants are highly hygroscopic, leading to awful moisture resistance ability of HTL and final devices.[11,23] In addition, the migration and diffusion of lithium ions (Li^+) within the whole device deteriorates light and thermal stabilities.[24,25] To address the instability induced by Li^+ diffusion, various types of strategies have been intensively investigated, chiefly including dopant-free hole transport materials (HTMs) (such as PM6,[26] TAT-2T-CAN,[27] PC3,[28] and P3HT[29]) and alternative dopants to Li-TFSI (e.g., $TBMP^+TFSI^-$[11] and $Zn\text{-}TFSI_2$[30]). Nevertheless, the devices using dopant-free HTMs or alternative LiTFSI dopants still exhibit inferior PCE than those based on Li-TFSI doping.[7,31] Therefore, it is imperative to develop new and efficient co-dopants to stabilize Spiro-OMeTAD HTL by suppressing Li^+ diffusion. It is well known that iodide ions (I^-) would diffuse from perovskite layer to interface between HTL and silver electrode, and the Ag atoms in metal electrode also would diffuse to perovskite layer through HTL.[25] The cross diffusion of Ag and I^- has been identified unambiguously as one main reason of degradation of PSCs.[32–34] In short, the migration and diffusion of Li^+, I^- and Ag in different functional layers greatly hinders the further development of regular PSCs. Except for stability, interfacial trap-assisted nonradiative recombination and relatively low conductivity of HTL would reduce the PCE of PSCs.

To date, significant efforts have been made to address these critical challenges, and substantial progress has been achieved. For example, Wang et al. incorporated 4-methanesulfonylbenzamidine hydrochloride (MSBH) at perovskite/Spiro-OMeTAD interface, and demonstrated that the migration of Li^+ ions was effectively inhibited via the strong coordination of sulfonyl group in MSBH with Li^+.[35] Furthermore, Li et al. introduced 12-Crown-4 in Spiro-OMeTAD HTL and demonstrated that 12-Crown-4 can suppress Li^+ migration through a host–guest interaction, thereby significantly enhancing moisture and thermal stability.[24] Yang et al. modified the HTL/Ag interface with molybdenum oxide ($HxMoO_3$) to limit Ag diffusion.[36] Our group developed a molecular locking strategy to stabilize perovskite/HTL interface by suppressing I^- migration and passivating undercoordinated Pb^{2+} defects using the polydentate ligand green biomaterial 2-deoxy-2,2-difluoro-d-erythro-pentafuranous-1-ulose-3,5-dibenzoate (DDPUD).[17] However, the above methods only inhibit the migration of Li^+, Ag or I^-. Recently, to enhance the functionality of molecular modulator, our group used L-glutamic acid dibenzyl ester 4-toluenesulfonate (GADET) to stabilize HTL and perovskite/HTL interface.[25] We demonstrated that the coordination of p-toluene sulfonate with Li^+ inhibits the migration of Li^+, and the $-NH_3^+$ in the molecule can form hydrogen bonds with I^- to inhibit the migration of I^-. Nonetheless, it remains challenging to simultaneously suppress the migration of Li^+, I^- and Ag by one simple and effective approach considering these mobile species originate from three distinct functional layers. Directly incorporating co-dopants into the HTL may offer a feasible and effective solution to simultaneously address the above challenges. The undercoordinated Pb^{2+} and/or halide vacancy defects can provide pathways for the migration of iodide ions. Iodide migration can be suppressed by passivating undercoordinated Pb^{2+} and/or halide vacancy defects.[17] The host–guest complexation strategy has been proposed to passivate undercoordinated Pb^{2+} defects,[37–40] suppressing Li^+ migration,[24,41] modulating perovskite crystallization[39,42] or stabilizing perovskite precursor solution.[33] However, at present, there are no reports on the simultaneous inhibition of Li^+, I^- and Ag migration by host–guest complexation, which indicates that the functionality of the host–guest complexation strategy still needs to be further expanded to fully realize its potential in multiple ion migration regulation. Given that active mobile chemical species such as Ag, Li^+ and undercoordinated Pb^{2+} are electron-deficient Lewis acid, developing a Lewis base ligand with strong coordination ability to effectively coordinate with these mobile ions should be able to achieve simultaneous inhibition of multilayer multiple mobile chemical species, thereby improving the long-term stability of PSCs. In consequence, it should be viable that Lewis base ligands can be utilized to concurrently inhibit the migration of Li^+, I^- and Ag via host–guest complexation interaction.

In this work, we proposed a multifunctional host–guest complexation strategy by incorporating a Lewis base ligand, bis(2,4,6-trichlorophenyl) oxalate (TCPO), into the Spiro-OMeTAD HTL. Through host–guest complexation interactions, TCPO can simultaneously suppress the migration and diffusion of Li^+, I^- and Ag, which stabilizes the perovskite layer, HTL and silver electrode along with their interfaces. In addition, the doping process of Spiro-OMeTAD was facilitated by adding TCPO, promoting hole extraction and transfer. Due to reduced surface defects, trap-induced nonradiative recombination was minimized. The introduction of two hydrophobic trichloro phenyl groups strengthened the moisture resistance of HTL and protected underlying perovskite films from invasion by moisture in ambient air. The devices doped with TCPO achieved a champion PCE of 25.68 % (certified 25.59 %). The unencapsulated TCPO doped devices only decayed by 9.98 % after continuous operation for 730 h at maximum power point (MPP) under one sun, and maintained 94.1 % of the initial efficiency after aging for 2800 h in ambient air with 30 % relative humidity (RH), which represents one of the best stabilities reported for regular PSCs. This study significantly improved the stability of n-i-p devices and lays a solid foundation for subsequent related research and commercial applications. This work provides a valuable reference and guidance for enhancing the photovoltaic performance and long-term stability of PSCs through a host–guest complexation strategy via the rational design of multifunctional Lewis base ligand molecules.

Results and Discussion

Theoretical Investigation of Inhibition Mechanisms of Mobile Li^+ Ions

In order to realize host–guest complexation interactions, we designed and selected the TCPO ligand molecules which possess a strong coordination ability with metal ions or atoms. TCPO consists of two structural units, namely 1,3,5-trichlorophenyl and oxalate. Meanwhile, oxalic acid (OA) and 1,3,5-trichlorobenzene (TCB) were used as reference molecules to elucidate the design rationale of TCPO ligands and highlight the synergistic effect of 1,3,5-trichlorophenyl and oxalate parts. Figure 1a shows the electrostatic potential (ESP) distribution of TCB, OA, and TCPO molecules. It can be observed that the potential of TCPO concentrates on the two carbonyls (C=O) while the potential on the two 1,3,5-trichlorophenyl groups is relatively low. It is inferred that the C=O in TCPO can strongly coordinate with Li^+ ions, undercoordinated Pb^{2+}, or Ag. Although the electron cloud density of C=O in OA is very high, the –OH in its structure also shows a high positive potential, which may have a repulsive interaction toward positively charged metal ions and thus weakens the coordination ability of C=O groups. The introduction of the two hydrophobic 1,3,5-trichlorophenyl groups on oxalate may enhance the coordination ability of C=O and improve the moisture resistance of the HTL and perovskite films.

To further verify our conjecture, density functional theory (DFT) calculations were used to explore the interaction of TCB, OA, or TCPO with Li^+, and the binding energy (E_b) was calculated (Figure 1b, c). As shown in Figure 1c, the E_b values of TCB-Li, OA-Li and TCPO-Li are 0.52, 2.32 and 2.51 eV, respectively. Obviously, TCPO has the highest binding energy with Li and forms the strongest chemical bond.[6] This confirms that the –OH on OA molecules may repel Li^+ and impair the interaction of C=O with Li^+, affirming that our ligand molecular design is legitimate. The design rationale of the target ligand molecule TCPO is exhibited in Figure 1d. TCB and OA molecules have their own advantages and disadvantages when used as co-dopants for Spiro-OMeTAD. The advantages of TCB are its large molecular weight and strong hydrophobicity. When it binds to Li^+, this large molecular weight can slow down the migration rate of Li^+, and its hydrophobicity can enhance the humidity stability of the HTL and the final device. Its disadvantage is relatively low electron cloud density, which leads to a very weak binding with Li^+. In contrast, the advantage of OA is high electron cloud density, which provides a very strong binding with

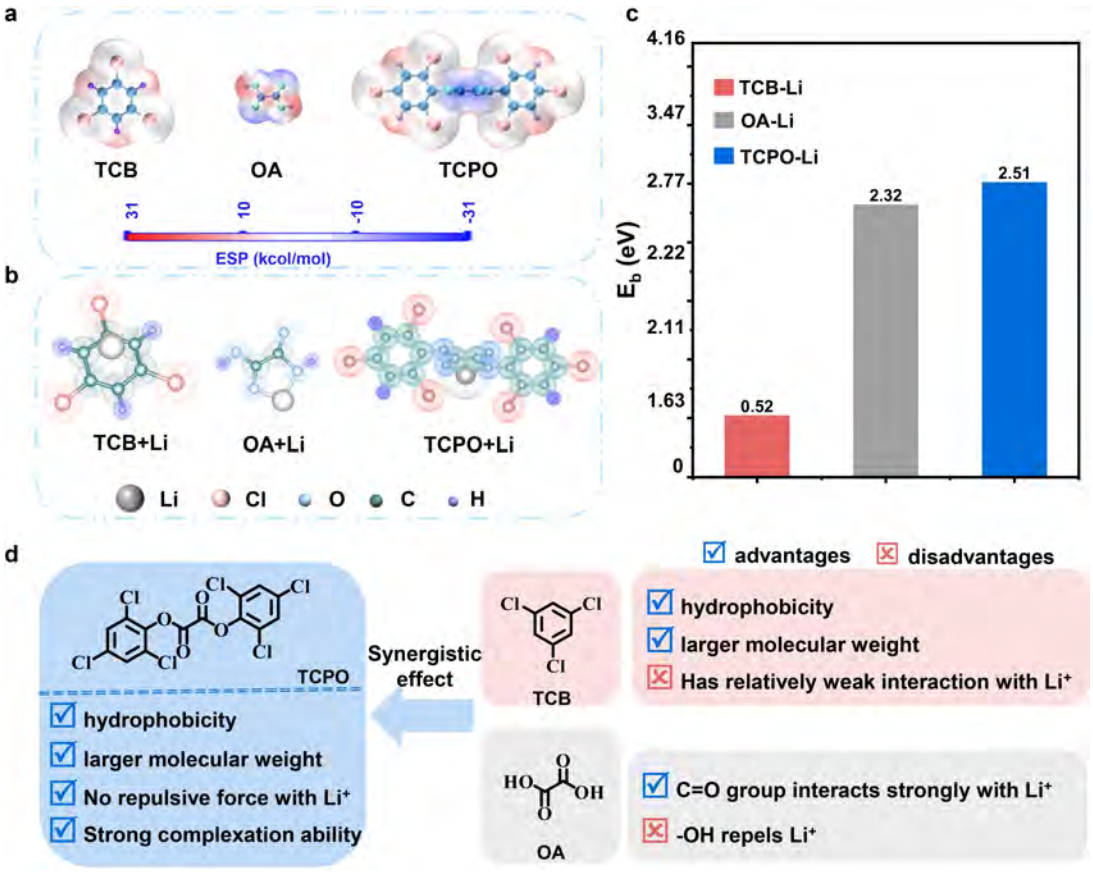

Figure 1. Theoretical insights into inhibition mechanisms of mobile Li^+ ions. (a) ESP images of TCB, OA, and TCPO. Molecular structures (b) and binding energies (c) of Li^+ with TCB, OA, and TCPO calculated and optimized using density functional theory. (d) Design thought of TCPO ligand molecules used for host–guest complexation interaction.

Li^+. However, the –OH in OA molecule also has a very high positive charge, which can repel Li^+. In view of this, we selected carefully TCPO molecules by combining the advantages of TCB and OA while avoiding their disadvantages. In a word, TCPO owns the following multiple advantages. First, TCPO molecule is large enough, so its migration rate will be greatly slowed down after binding with Li^+. Second, the electron cloud density of C=O in TCPO is sufficiently high, making it firmly bound to Li^+. Finally, the incorporation of the TCB structural units may enhance the hydrophobicity of TCPO while reinforcing its binding ability with Li^+ and avoiding the repulsive force of –OH toward Li^+. To sum up, it is justifiable to choose TCPO as the target p-dopant to achieve host–guest complexation with metal ions and atoms.

Promoted p–doping and chemical interaction mechanisms

We subsequently investigated the effect of TCPO on the p-doping process and its chemical interaction with Li^+. For ease of description, henceforward, Spiro-OMeTAD was abbreviated as Spiro. The Spiro solutions and films doped by TCPO, doped by Li-TFSI and *t*-BP, and doped by Li-TFSI, *t*-BP and TCPO were denoted as Spiro, Spiro-TCPO, Spiro-Li, and Spiro-Li-TCPO, respectively. We observed that adding the co-dopant TCPO to the fresh Spiro-Li solution induced a color change (Figure S1), which could be ascribed to the coordination interaction between TCPO and Li^+. For Spiro and Spiro-TCPO solutions, no color change was observed even when aging time was extended to 7 days, while the color of Spiro-Li and Spiro-Li-TCPO solutions darkened. Moreover, a more significant color change was found in Spiro-Li-TCPO compared to Spiro-Li. This indicates that TCPO itself could not dope Spiro but can indirectly facilitate its oxidation. In addition, electron spin resonance (ESR) was used to detect the free radical content in the HTL solution (Figure 2a). It can be seen that no paramagnetic peaks appeared in the spectra of Spiro and Spiro-TCPO solutions, suggesting that there are no free radicals or their concentration is extremely low.[43] By contrast, Spiro-Li and Spiro-Li-TCPO showed strong para-

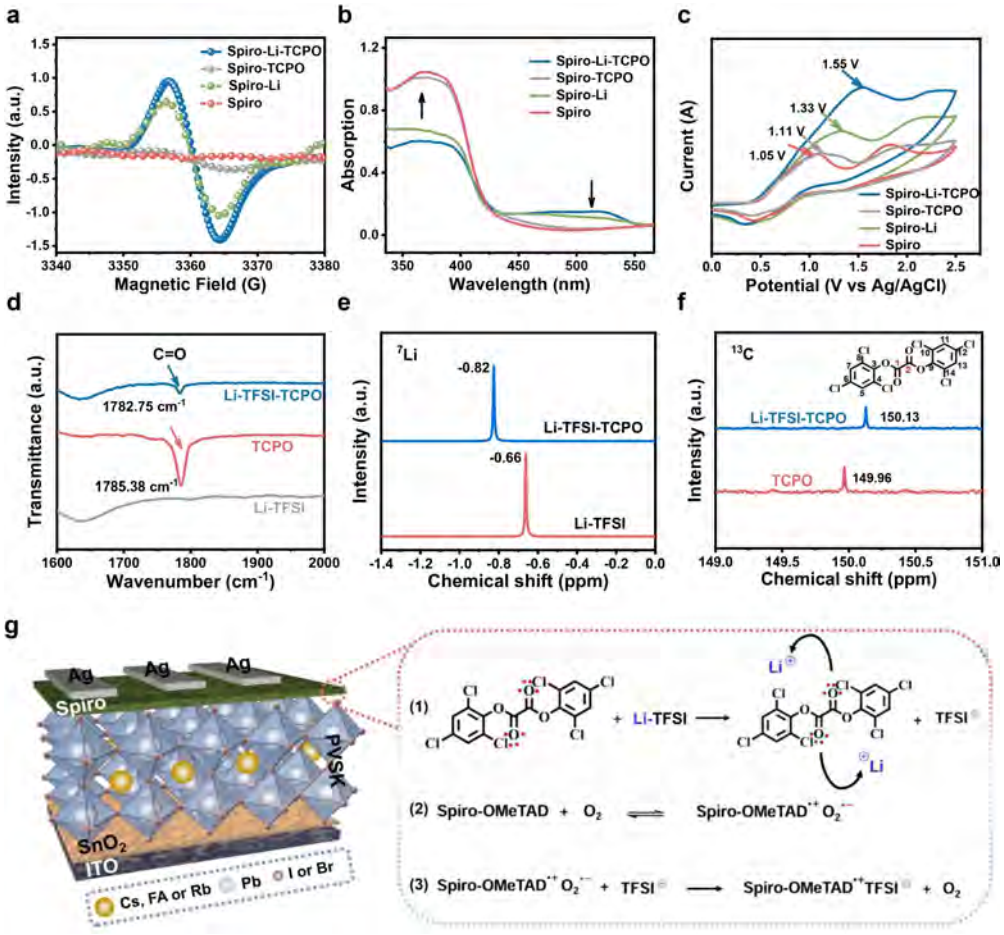

Figure 2. Promoted p-doping by TCPO and chemical interaction of TCPO with Li^+ ion. (a) ESR spectra of Spiro, Spiro-TCPO, Spiro-Li, and Spiro-Li-TCPO solutions. (b) UV/Visible absorption spectra of Spiro, Spiro-TCPO, Spiro-Li and Spiro-Li-TCPO films. (c) Cyclic voltammograms of Spiro, Spiro-TCPO, Spiro-Li, and Spiro-Li-TCPO. (d) FTIR spectra of Li-TFSI, TCPO and TCPO-Li-TFSI in the wavenumber range of 1600–2000 cm^{-1}. (e) ^7Li NMR of Li-TFSI solutions with and without TCPO. (f) ^{13}C NMR of TCPO solutions with and without Li-TFSI. (g) Schematic illustration of the mechanisms of p-doping promotion and Li^+ migration suppression via TCPO.

magnetic peaks at 3350–3370 G, indicating the presence of significant amounts of Spiro$^{\bullet+}$.[44] It is worth noting that the Spiro-Li-TCPO solution showed a stronger peak signal compared to Spiro-Li. The above results confirm that TCPO did not directly participate in the p-doping process but indirectly promoted the oxidation of Spiro by Li-TFSI. We further verified the ability of TCPO as a co-dopant by UV/Visible (UV/Vis) spectroscopy. For Spiro and Spiro-TCPO samples, no peak of the oxidation product Spiro$^{\bullet+}$ at ~520 nm appeared,[45] further proving the results of ESR that TCPO could not react with Spiro. In Spiro-Li and Spiro-Li-TCPO, the oxidation characteristic peak appeared. It is worth noting that the intensity of the characteristic peak of Spiro$^{\bullet+}$ in Spiro-Li-TCPO is the strongest, suggesting that TCPO had a complex interaction with Li^+, thereby promoting the oxidation of Spiro (Figure 2b). The change in the position of the UV peak only serves as a proof of the promotion of Spiro oxidation products, and cannot confirm that the light absorption of the material has changed. In Figure 2c, we further explored the reason for the high oxidation ability of Spiro-Li-TCPO using cyclic voltammetry (CV). The results show that the first oxidation potentials of Spiro, Spiro-TCPO, Spiro-Li and Spiro-Li-TCPO are 1.05, 1.11, 1.33 and 1.55 V, respectively. The potential difference between Spiro and Spiro-TCPO is essentially negligible, which further shows that TCPO had no obvious oxidation effect on Spiro. However, the potential difference between Spiro-Li and Spiro-Li-TCPO increased markedly, indicating that the co-doping of TCPO raised the oxidation potential of Spiro-Li. This renders Spiro-Li-TCPO more susceptible to single-electron oxidation reactions, accelerating the oxidation of spiro.[25] This is also why the above-mentioned Spiro-Li-TCPO solution exhibits more significant color changes. As mentioned above, TCPO can effectively promote the oxidation of Spiro in the presence of Li-TFSI, but its chemical mechanism needs further clarification. As shown in Figure 2d and Figure S2a, in TCPO, the peak of C=O was located at 1785.38 cm^{-1}, while Li-TFSI lacks this peak. After adding Li-TFSI to TCPO, the carbonyl peak position shifted by 2.63 cm^{-1}, indicating that the C=O formed an interaction with Li-TFSI.[46] The infrared spectra of TCPO and Spiro-TCPO show that the C=O peak did not move (Figure S2b, c). To further study the chemical interaction between TCPO and Li-TFSI, the ^{7}Li nuclear magnetic resonance (NMR) spectra of TCPO-Li-TFSI and Li-TFSI solution were collected, as shown in Figure 2e. Obviously, the addition of TCPO led to the shielding of Li^+ ions, because the electron-donating functional group C=O in TCPO provided electrons to lithium ions, causing the Li^+ peak to move to the high field.[47] To further prove this, ^{13}C NMR was used to examine changes in the chemical environment of C atoms (Figure 2f). The peak position in the Li-TFSI-TCPO sample showed a significant chemical shift compared to pure TCPO, demonstrating that the addition of Li-TFSI changed the chemical environment of C atoms on C=O in TCPO. Specifically, the electrons on C=O in TCPO partially transferred to the vicinity of Li^+ and thus neutralized part of the positive charge of Li^+, which resulted in a decrease in the electron cloud density on the carbon atom and a weakening of the shielding effect around the carbon, thereby causing its chemical shift to move to the low field.[25] It can be concluded from the above FTIR and NMR results that the TCPO interacted with Li-TFSI via the coordination bond between C=O and Li^+.

Based on the above results, a possible chemical mechanism was proposed (Figure 2g). Upon incorporating TCPO as co-dopant in HTL, more $TFSI^-$ anions can be dissociated from Li-TFSI molecules because of host–guest complexation interaction between TCPO and Li^+. The generated more $TFSI^-$ anions can react with unstable oxidized product Spiro$^{\bullet+}O_2^{\bullet-}$ to form stable Spiro$^{\bullet+}TFSI^-$, which made the oxidation reaction of Spiro proceed toward the forward direction, thereby promoting the oxidation of Spiro. We can draw a conclusion that TCPO indirectly takes part in the p-doping process and expedites the oxidation of Spiro.

Characterization of HTLs without and with TCPO

We tested the electrical properties of HTLs containing different dopants at their optimal doping concentration to evaluate their hole transport capabilities. As shown in the atomic force microscopy (AFM) image in Figure 3a, the root mean square roughness (RMS) of all doped films was lower than that of the pristine Spiro. From the conductive atomic force microscopy (c-AFM) image (Figure 3b), it can be seen that the average current values of Spiro-Li (10.91 pA) and Spiro-Li-TCPO films (13.23 pA) were significantly higher than that of Spiro (5.14 pA) and Spiro-TCPO (6.86 pA) films. Among these, the Spiro-Li-TCPO film had the highest average current value and the most uniform current distribution. These observations are also consistent with the corresponding film conductivity results (Figure 3c and Figure S3). At the same time, we also tested the hole mobility of the Spiro film to examine the charge transport performance. As shown in Figure 3d and Figure S4, the hole mobility of Spiro-Li-TCPO (2.77×10^{-3} cm^2 V^{-1} S^{-1}) is significantly higher than that of the undoped Spiro (1.12×10^{-3} cm^2 V^{-1} S^{-1}), Spiro-TCPO (1.16×10^{-3} cm^2 V^{-1} S^{-1}) and Spiro-Li (1.97×10^{-3} cm^2 V^{-1} S^{-1}). The host–guest complexation between TCPO and Li^+ facilitated the oxidation of Spiro, which is likely mainly responsible for the improved conductivity and hole mobility.

Subsequently, we evaluated the effect of TCPO doping on interfacial hole extraction and transfer by performing steady-state photoluminescence (PL) and time-resolved photoluminescence (TRPL) spectra measurements (Figure 3e, f and Table S1). Compared with the perovskite/Spiro-Li, the perovskite/Spiro-Li-TCPO exhibited a lower PL intensity and shorter carrier lifetime, implying that hole extraction was enhanced after TCPO co-doping due to the improved electric properties of HTL and better energy band alignment. The energy level values of Spiro-Li and Spiro-Li-TCPO films were measured and calculated (Figure S5–7 and Table S2). As illustrated in Figure 3g, the TCPO doping led to smaller energy level offset between the valence band maximum (VBM) of perovskite film and highest occupied molecular orbital (HOMO) of HTL, which promoted the

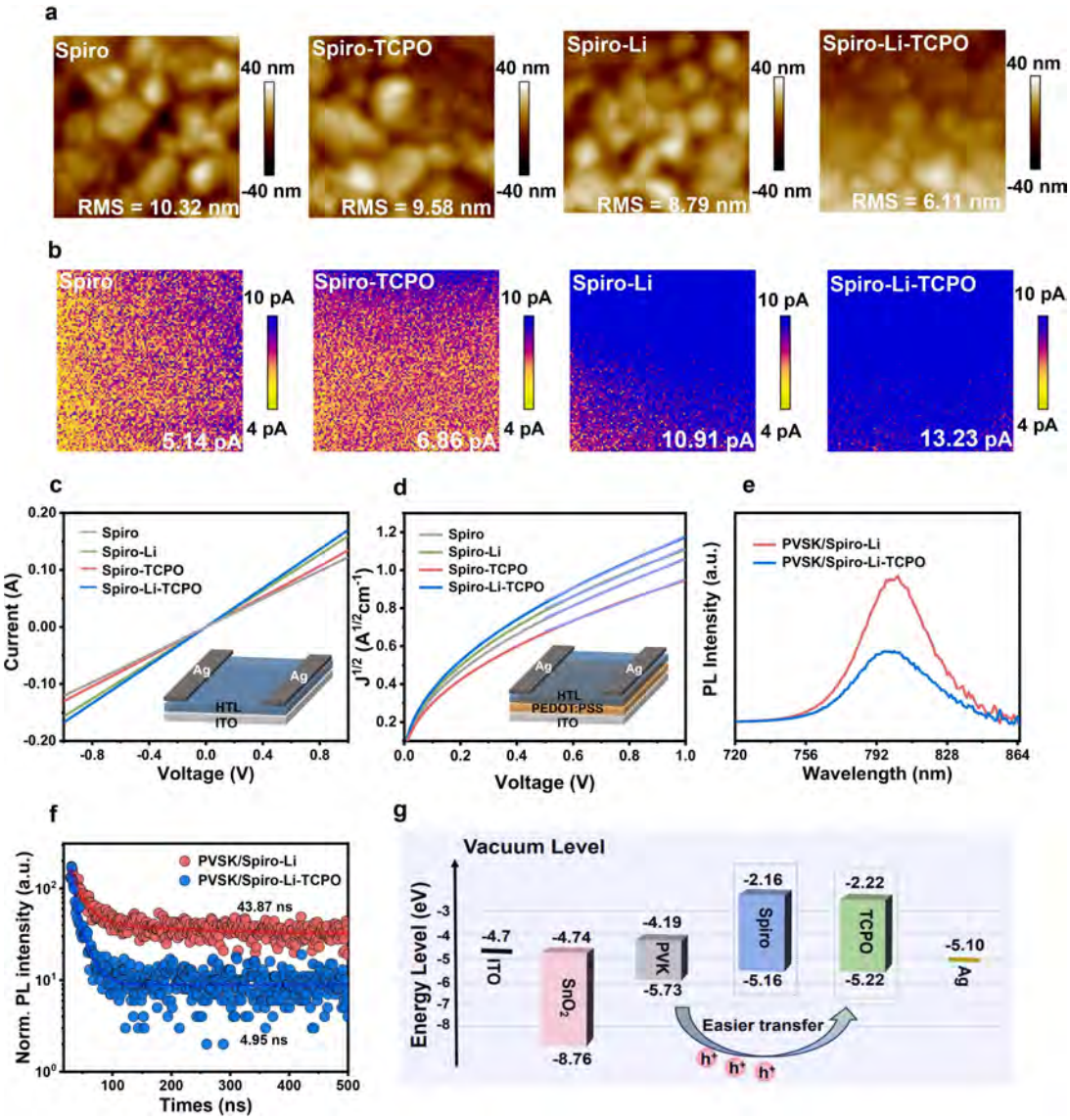

Figure 3. Characterization of HTLs without and with TCPO. AFM (a) and c-AFM (b) images of pure Spiro, Spiro-TCPO, Spiro-Li, and Spiro-Li-TCPO. The size of the images is 2×2 μm^2. Conductivities (c) and hole mobilities (d) of pure Spiro, Spiro-TCPO, Spiro-Li, and Spiro-Li-TCPO. PL (e) and TRPL (f) spectra of perovskite films coated with Spiro-Li and Spiro-Li-TCPO films on glass substrates. PVSK stands for perovskite. (g) Energy level arrangement of Spiro-Li films with and without TCPO.

extraction of interface holes and reduced the interface non-radiative recombination loss.

Passivation of Perovskite Film Surface with TCPO

As a dopant in HTL, TCPO will inevitably contact the upper interface of the perovskite films. Consequently, we also investigated the passivation effect of TCPO on the top surface of perovskite films. The infrared spectra in Figure S8a–b and the XPS spectra in Figure S8c show that C=O groups in TCPO can coordinate with Pb^{2+}. After TCPO modification, the PL intensity and carrier lifetime of perovskite films increased significantly (Figure S9a, b and Table S3), demonstrating that TCPO can effectively passivate the undercoordinated Pb^{2+} defects at the surface of perovskite films through host–guest complexation with undercoordinated Pb^{2+}. As presented in Figure S9c, d, TCPO treatment resulted in a decrease in defect density from 1.06×10^{16} cm^3 to 7.24×10^{15} cm^3, likely due to effective passivation of undercoordinated Pb^{2+} and/or iodide vacancy defects. Since iodide ions migrate along these pathways, passivation of these defects can inhibit iodide ion migration, thus enhancing the intrinsic durability of PSCs, which will be corroborated in the next moment.

Simultaneous Suppression of Li^+, I^- and Ag Migration

To accurately and objectively gain insights into the effect of the addition of the co-dopant TCPO on the stability of the functional layers and devices, we carried out accelerated damp-heat and photothermal aging tests under relatively harsh conditions. Because the actual temperature of PSCs under normal operation can reach ~65 °C,[48] we set more stringent conditions to test our devices. The damp-heat aging test conditions involved heating the perovskite films with Spiro-Li (control) and Spiro-Li-TCPO (target) at 85 °C under an ambient RH of 61 % (Figure 4a). After aging for 8 days, we observed the formation of a large amount of yellow PbI_2 and the green color of HTL completely disappeared in the control sample. In comparison, almost no PbI_2 was visible to the naked eye in the target sample under the same aging conditions, indicating that the control sample degraded much more rapidly than the target sample. This suggests that the moisture resistance of HTL and perovskite films were significantly enhanced after TCPO doping, which is put down to the strong hydrophobicity of TCPO containing two hydrophobic trichloro phenyl segments. After adding TCPO, Figure 4b shows that the water contact angle of HTLs was much increased from 67.57° to 78.07°, which accounts for reinforced moisture stability of the HTL and perovskite film. We also measured the scanning electron microscope (SEM) images for the fresh and aged control and target samples under the conditions of 65 % RH and 85 °C (Figure 4c). The SEM images show that after 8 days of aging of the control sample, the HTL completely collapsed and the perovskite layer was partially degraded, which is hygroscopicity of Li-TFSI and *t*BP as well as the aggregation and diffusion of Li^+. By comparison, the HTL partially degraded and the perovskite films almost did not decompose for the target sample. In short, the introduction of TCPO dopant dramatically heightened the moisture tolerance of HTL and underlying perovskite film.

Then, the time-of-flight secondary ion mass spectrometry (TOF-SIMS) measurement was adopted to investigate the intrinsic stability of PSCs by analyzing cross-sectional distribution of Li^+, I^- and Ag. For the control device, after aging for 8 days under 85 °C and one sun illumination, a significant amount of Li^+ ions had diffused to the Ag electrode and perovskite layer, while Ag had diffused into the HTL and perovskite layer, and a large amount of I^- migrated to the Ag layer (Figure 4d and Figure S10). It can be seen that the Li^+ concentration in the HTL layer of the target device is higher than that of HTL in the control device, while the concentration trend of Li^+ accumulation in other layers is reversed. Although I^-, Li^+ and Ag also diffused in the target device, the diffusion in the target device is much less significant than that in the control device. This diffusion behavior is clearly illustrated in Figure 4e. The ion migration and diffusion in the control and target devices is schematically depicted in Figure 4f. In the control device, Li^+ would easily diffuse to Ag and perovskite layers. At the same time, the cross diffusion of Ag and I^- is easy to occur. When TCPO was employed as co-dopant in HTL, it possessed the following several functions. First, as discussed above, TCPO doping can significantly reinforce the moisture stability of HTL and underneath perovskite film. Second, it can suppress the migration of Li^+ via the host–guest complexation between TCPO and Li^+. Third, the migration of I^- can be effectively inhibited by host–guest complexation of TCPO with under-coordinated Pb^{2+}. Finally, the host–guest complexation between TCPO and Ag can restrain the diffusion of Ag electrode. In conclusion, these findings demonstrate that TCPO doping can simultaneously suppress the diffusion and migration of Li^+, I^- and Ag, thereby contributing to enhancing long-term operational stability of PSCs.

Photovoltaic Performance

We prepared the regular devices based on Spiro and Spiro-TCPO HTLs. The results show that the efficiency for 2.5 mg/ml TCPO is 7.5 %, while the efficiency for pure Spiro is 5.3 %, both of which are much lower than the efficiency of Spiro-Li devices (Figure S11 and Table S4). As previously discussed, TCPO cannot directly dope the Spiro without the presence of Li-TFSI and *t*BP. The slight improvement in the efficiency of Spiro-TCPO device relative to the Spiro device is likely due to the decrease in the roughness of the HTL and the enhancement of the hole transport ability. It is again reliable to conclude that TCPO can only coordinate with Li^+ to promote the dissociation of $TFSI^-$, thereby accelerating the oxidation of Spiro instead of directly oxidizing Spiro alone.

To investigate the effect of HTL layer modification on the performance of planar regular devices, we constructed complete devices with Spiro-Li-TCPO, Spiro-Li-OA and Spiro-Li-TCB as HTL layers. Unless emphasized, the effective active area of all devices was 0.1 cm^2 and perovskite composition was $Rb_{0.02}(FA_{0.95}Cs_{0.05})_{0.98}PbI_{2.91}Br_{0.03}Cl_{0.06}$.[49] The optimal doping concentration for TCPO, OA and TCB was 1.0, 0.5, and 0.5 mg/mL, respectively (Figures S12–S14 and Tables S5–S7). The device performance statistics shown in the box plots in Figures S12–14 clearly indicate that there are no outliers in the dataset. In addition, the standard deviations of the efficiency data in Tables S5–S7 are small (0.219–0.437), which means that the values deviate from the mean value and the experimental error is small. Although the photovoltaic performance was increased for all dopants compared with the device based on Spiro-Li, as expected, TCPO based devices exhibited the most notable performance, which is because of the combination of the advantages of TCB and OA as mentioned above. Figure 5a shows the champion *J*–*V* curves of the control (based on Spiro-Li) and target (based on Spiro-Li-TCPO) devices. The PCE of the control device is 23.01 %, corresponding to an open-circuit voltage (V_{oc}) of 1.166 V, a short-circuit current density (J_{sc}) of 24.12 mA/cm^2, and a fill factor (FF) of 0.819. The PCE of the target device was much improved to 25.07 % with a V_{oc} of 1.182 V, a J_{sc} of 25.16 mA/cm^2, and an FF of 0.843. Obviously, all photovoltaic parameters were ameliorated, which is ascribed to significantly reduced nonradiative

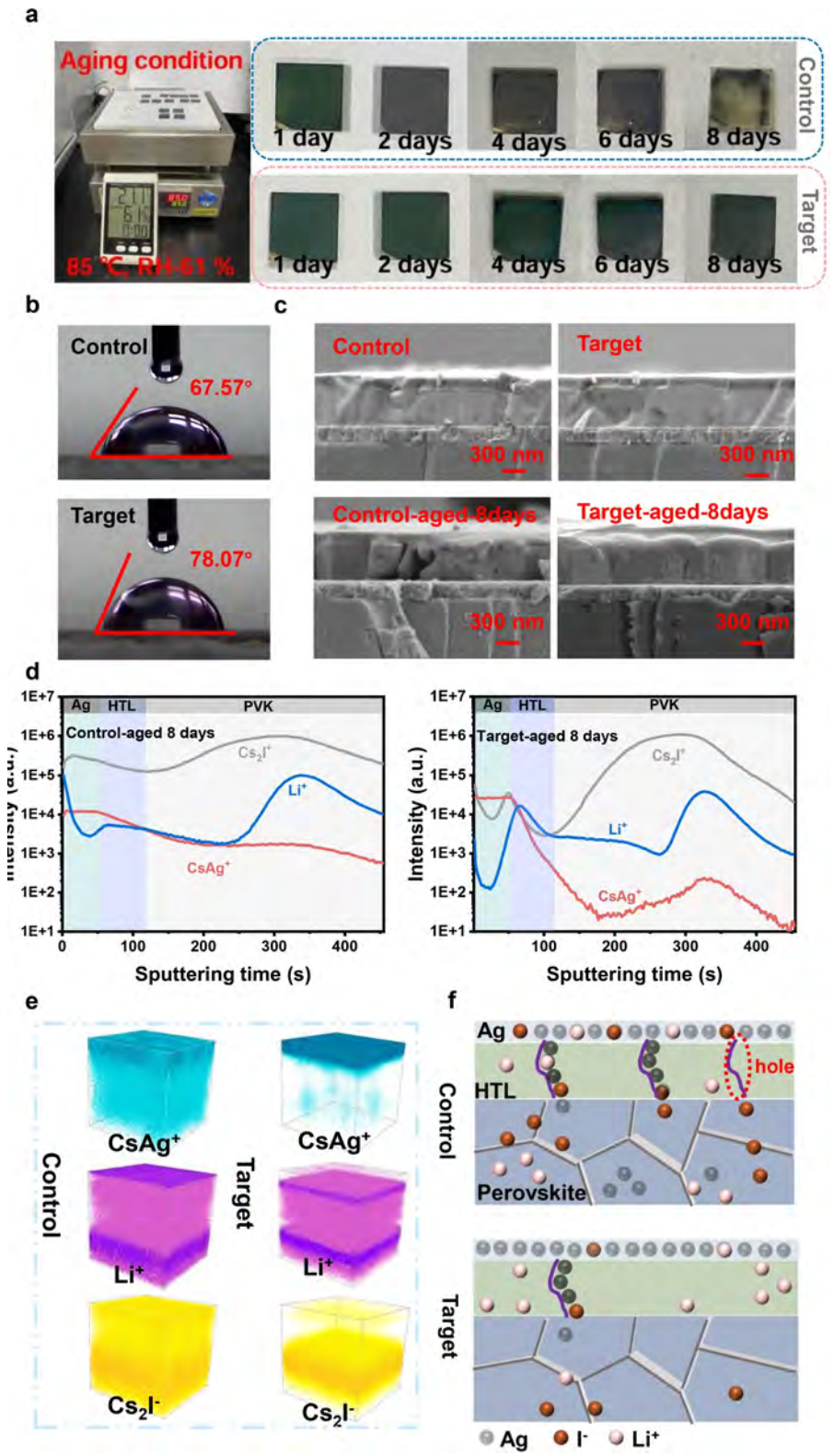

Figure 4. Simultaneous suppression of Li^+, I^- and Ag migration via host–guest complexation. (a) Photographs of the perovskite films with Spiro-Li (control) and Spiro-Li-TCPO (target) under damp and heat environment (temperature 85 °C, relative humidity 61 %) after aging for 1, 2, 4, 6 and 8 days. (b) Water contact angles of the perovskite films with Spiro-Li and Spiro-Li-TCPO. (c) Cross-sectional SEM images of the perovskite films with Spiro-Li and Spiro-Li-TCPO under damp and heat environment (temperature 85 °C, relative humidity 61 %) before and after aging for 8 days. (d) TOF-SIMS for the control and target devices after exposing to one sun and heating at 65 °C for 8 days. (e) TOF-SIMS 3D reconstruction of $CsAg^+$, $Cs_2I^-$and Li^+ ions. (f) Schematic diagram of suppressing I^-, Li^+, and Ag migration through TCPO.

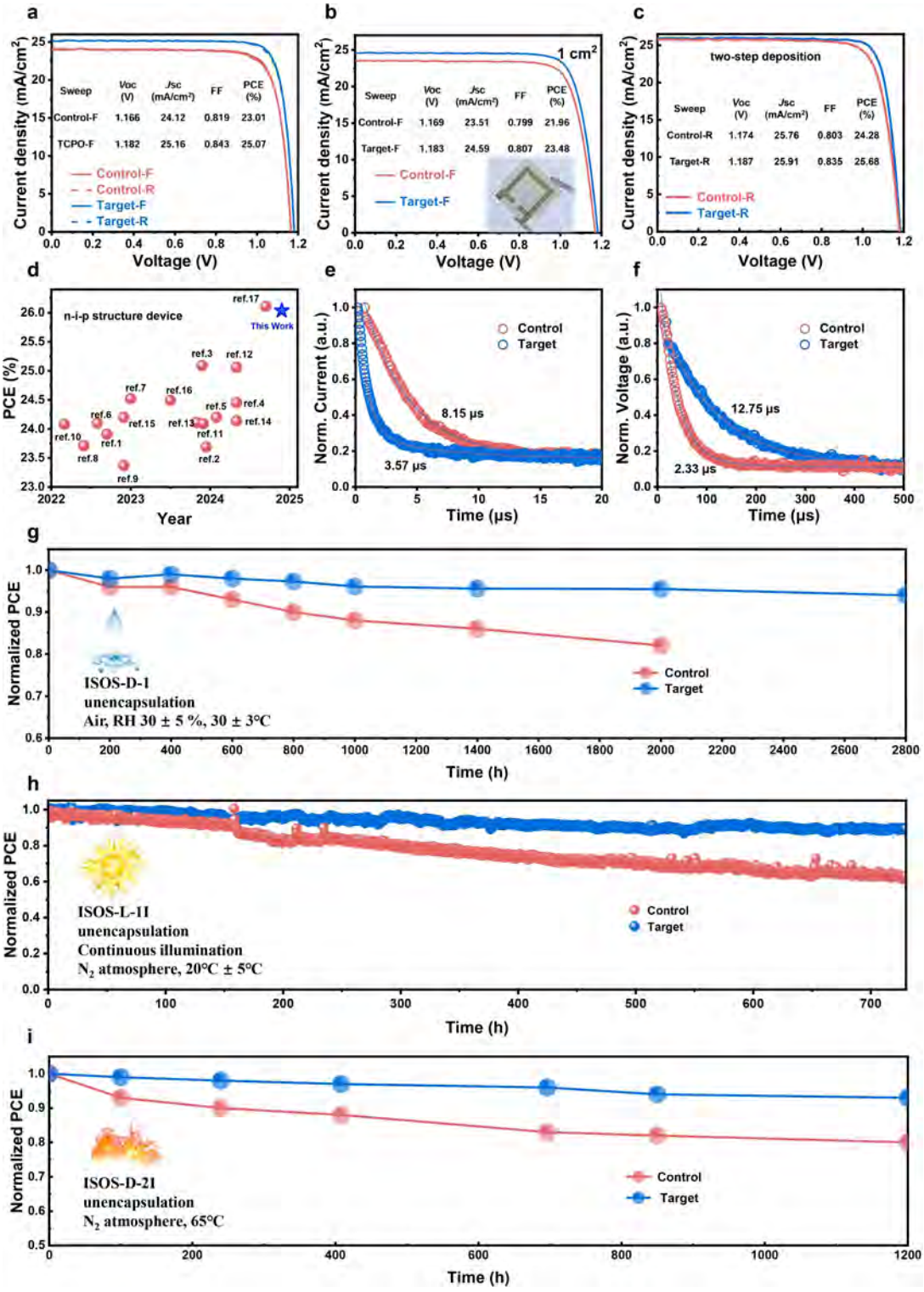

Figure 5. Photovoltaic performance and long-term stability of devices without and with TCPO. (a) *J–V* curves of the best-performing devices without and with TCPO. (b) *J–V* curves of the champion control and target devices with an active area of 1 cm^2. (c) *J–V* curves of the best-performing devices without and with TCPO prepared using a two-step perovskite deposition approach (active area 0.08 cm^2). (d) Comparison of the PCEs for our device and reported highly efficient n-i-p structure PSCs. TPC (e) and TPV (f) curves for the control and target devices. (g) Humidity stability of the control and modified PSCs in a light-shielded environment at 25–35 % relative humidity. (h) Operation stability of the unencapsulated control and target devices at MPP under continuous 1 sun irradiation. (i) Thermal stability of the unencapsulated control and modified devices heated at 65 °C in a dark nitrogen glove box.

recombination resulting from enhanced conductivity and hole mobility of HTL along with more favorable energy level alignment. For comparison, the PSCs with Spiro-Li-OA and Spiro-Li-TCB achieved a lower PCE of 23.88 % and 23.53 %, respectively (Figure S15a and b). Figure S16 illustrates the external quantum efficiency (EQE) spectra and the integrated current density of the control and target devices. The calculated integrated current density of the control and target device is 23.28 mA/cm^2 and 24.52 mA/cm^2, respectively, which is consistent with the values extracted from *J–V* curves. Importantly, our doping technology was also used to fabricate large-area PSCs with an active area of 1 cm^2, resulting in a marked PCE enhancement from 21.96 % to 23.48 % (Figure 5b).

In addition, we also confirmed the universality of our multifunctional molecular complexation strategy by fabricating regular planar PSCs based on a two-step perovskite deposition method. The champion *J–V* curves of the control and target devices are shown in Figure 5c. After TCPO modification, the PCE increased significantly from 24.28 % to 25.68 %, demonstrating the broad applicability of our molecular complexation strategy for various perovskite compositions. The best-performing target PSC was certified by an independent solar cell certification laboratory (China National Institute of Metrology) with a PCE of 25.59 % with a V_{oc} of 1.179 V, a J_{sc} of 26.57 mA/cm^2, and an FF of 81.72 % (Figure S17), which is one of the highest PCE ever reported for the n-i-p structure PSCs (Figure 5d and Table S8).

To study the contribution of TCPO passivation to the enhanced photovoltaic performance, we prepared regular devices by directly applying TCPO to treat the surface of perovskite films. The device treated with TCPO as an upper interface modifier demonstrated a PCE of 23.85 %, which is higher than 23.01 % of the device without TCPO treatment, confirming the defect passivation ability of TCPO (Figure S18a). To further demonstrate the universality of our host–guest complexation strategy, we also prepared PSCs based on $FAPbI_3$ as the photoactive layer with and without TCPO-doped HTLs. After TCPO modification, the PCE improved from 21.80 % to 23.33 %, affirming the generality of our molecular modulation strategy (Figure S18b).

The charge extraction and transfer process were additionally studied using transient photocurrent (TPC). Compared with the Spiro-Li device (8.15 μs), the carrier decay lifetime of the Spiro-Li-TCPO device (3.57 μs) was significantly reduced (Figure 5e). In addition, we used transient photovoltage (TPV) decay measurements to investigate the carrier recombination dynamics. As can be seen from Figure 5f, the Spiro-Li-TCPO device exhibited a longer decay lifetime, suggesting that the non-radiative recombination loss was minimized after modification. The improvements in V_{CO} and FF are attributed to the reduction in defect state density and suppressed non-radiative recombination. Additionally, the enhancement of hole mobility and conductivity of HTL as well as the improvement of energy band alignment are the main reasons for the increase in J_{sc}.

Long-Term Stability

Finally, we systematically explored the long-term stability of the devices based on Spiro-Li and Spiro-Li-TCPO under different aging conditions according to the International Summit on Organic Photovoltaic Stability (ISOS) protocols.[50] According to the ISOS-D-1 protocol, the ambient stability of the unencapsulated devices was tested under environmental conditions of ~30 °C and ~30 % RH. After 2800 h, the PCE of the control and target devices decreased to 94.1 % and 82.1 % of the initial value, respectively (Figure 5g), indicating improved moisture stability in the TCPO-doped device. The strong hydrophobicity of TCPO should be primarily responsible for much enhanced moisture resistance. Following the ISOS-L-1I protocol, we also examined the long-term operational stability of the unencapsulated devices under one sun illumination in a N_2 glove box (Figure 5h). The target device still retained about 90.02 % of its initial PCE after 730 h of operation. In contrast, the control device dropped to 62.80 % of its initial PCE. Both the control and target devices were subjected to thermal stability tests in nitrogen at 65 °C (ISOS-D-2I). The target device retained 93.0 % of its initial efficiency after 1200 h of heat aging, while the efficiency of the control device dropped to 80.2 % (Figure 5i). Overall, the incorporation of TCPO significantly improved thermal and light stabilities, which is mainly due to effective suppression of the migration and diffusion of Li^+, I^- and Ag by host–guest complexation with TCPO ligand molecules. Certainly, reduced interfacial defects and inhibited nonradiative recombination also make contribution to strengthened light and thermal stabilities. It can be concluded that our developed multifunctional host–guest complexation strategy enabled the simultaneous enhancement of photovoltaic performance and long-term durability due to the suppression of the migration and diffusion of Li^+, I^- and Ag and facilitated p-doping.

Conclusions

In summary, we developed multifunctional host–guest complexation strategy that bis(2,4,6-trichlorophenyl) oxalate (TCPO) was introduced into Spiro-OMeTAD hole transport layer (HTL). The host–guest complexation interaction made TCPO simultaneously suppress the migration and diffusion of Li^+, I^- and Ag, which significantly heightened the intrinsic stability of functional layers and the final devices. Moreover, TCPO modification can accelerate the oxidation of Spiro-OMeTAD, enhancing the conductivity and hole mobility of HTL. Increased hole mobility, favorable energy band alignment and diminished interfacial defects facilitated hole extraction and inhibited nonradiative recombination losses. The TCPO doped devices obtained a promising peak PCE of 25.68 % (certified 25.59 %, 0.08 cm^2) and 23.48 % (1 cm^2). After 730 h of continuous operation at MPP under one sun illumination, the unencapsulated TCPO doped devices maintained 90.0 % of its initial PCE. The unencapsulated TCPO doped devices demonstrated excellent ambient

stability, retaining 94.1 % of the initial efficiency after 2800 h of exposure to the ambient air with 30 % RH, which is one of the best stabilities reported for regular PSCs. This work provides deep insights into enhancing the photovoltaic performance and long-term stability of PSCs by host–guest complexation strategy via rational design of multifunctional ligand molecules.

Methods

Materials, Device fabrication, Characterization, and density functional theory details are given in the Supporting Information.

Acknowledgements

This work was financially supported by the National Natural Science Foundation of China (62274018), the Xinjiang Construction Corps Key Areas of Science and Technology Research Project (2023AB029), the Tianchi Talent Program of Xinjiang Uygur Autonomous Region (2024, Jiangzhao Chen) and the Key Project of Chongqing Overseas Students Returning to China Entrepreneurship and Innovation Support Plan (cx2023006).

Conflict of Interest

The authors declare no conflict of interest.

Data Availability Statement

The data that support the findings of this study are available from the corresponding author upon reasonable request.

Keywords: Perovskite solar cells · ion migration · p-doping · stability

[1] R. Tian, S. Zhou, Y. Meng, C. Liu, Z. Ge, *Adv. Mater.* **2024**, 2311473.
[2] C. Shen, T. Ye, P. Yang, G. Chen, *Adv. Mater.* **2024**, *36*, 2401498.
[3] S. Chaosukho, S. Meeklinhom, S. Rodbuntum, N. Sukgorn, A. Kaewprajak, P. Kumnorkaew, V. Varabuntoonvit, *Environmental Impact Assessment Review* **2024**, *106*, 107462.
[4] J. Zhang, X.-G. Hu, K. Ji, S. Zhao, D. Liu, B. Li, P.-X. Hou, C. Liu, L. Liu, S. D. Stranks, *Nat. Commun.* **2024**, *15*, 2245.
[5] N. A. N. Ouedraogo, G. O. Odunmbaku, Y. Ouyang, X. Xiong, B. Guo, S. Chen, S. Lu, K. Sun, *Renewable Sustainable Energy Rev.* **2024**, *192*, 114161.
[6] H. Chen, C. Liu, J. Xu, A. Maxwell, W. Zhou, Y. Yang, Q. Zhou, A. S. Bati, H. Wan, Z. Wang, *Science* **2024**, *384*, 189–193.
[7] M. J. Paik, Y. Y. Kim, J. Kim, J. Park, S. I. Seok, *Joule* **2024**, *8*, 2073–2086.
[8] J. Zhou, L. Tan, Y. Liu, H. Li, X. Liu, M. Li, S. Wang, Y. Zhang, C. Jiang, R. Hua, *Joule* **2024**, *8*, 1691–1706.
[9] S. Du, H. Huang, Z. Lan, P. Cui, L. Li, M. Wang, S. Qu, L. Yan, C. Sun, Y. Yang, *Nat. Commun.* **2024**, *15*, 5223.
[10] P. Shi, Y. Ding, B. Ding, Q. Xing, T. Kodalle, C. M. Sutter-Fella, I. Yavuz, C. Yao, W. Fan, J. Xu, *Nature* **2023**, *620*, 323–327.
[11] T. Zhang, F. Wang, H.-B. Kim, I.-W. Choi, C. Wang, E. Cho, R. Konefal, Y. Puttisong, K. Terado, L. Kobera, *Science* **2022**, *377*, 495–501.
[12] P. Chen, Y. Xiao, J. Hu, S. Li, D. Luo, R. Su, P. Caprioglio, P. Kaienburg, X. Jia, N. Chen, *Nature* **2024**, *625*, 516–522.
[13] S. Yu, Z. Xiong, H. Zhou, Q. Zhang, Z. Wang, F. Ma, Z. Qu, Y. Zhao, X. Chu, X. Zhang, *Science* **2023**, *382*, 1399–1404.
[14] S. Zhang, F. Ye, X. Wang, R. Chen, H. Zhang, L. Zhan, X. Jiang, Y. Li, X. Ji, S. Liu, *Science* **2023**, *380*, 404–409.
[15] H. Li, C. Zhang, C. Gong, D. Zhang, H. Zhang, Q. Zhuang, X. Yu, S. Gong, X. Chen, J. Yang, *Nat. Energy* **2023**, *8*, 946–955.
[16] Z. Zhang, M. Li, R. Li, X. Zhuang, C. Wang, X. Shang, D. He, J. Chen, C. Chen, *Adv. Mater.* **2024**, 2313860.
[17] B. Liu, X. Ren, R. Li, Y. Chen, D. He, Y. Li, Q. Zhou, D. Ma, X. Han, X. Shai, J. Chen, *Adv. Mater.* **2024**, 2312679.
[18] S. Teale, M. Degani, B. Chen, E. H. Sargent, G. Grancini, *Nat. Energy* **2024**, *9*, 779–792.
[19] Q. Jiang, K. Zhu, *Nat. Rev. Mater.* **2024**, 1–21.
[20] S. M. Park, M. Wei, J. Xu, H. R. Atapattu, F. T. Eickemeyer, K. Darabi, L. Grater, Y. Yang, C. Liu, S. Teale, *Science* **2023**, *381*, 209–215.
[21] B. Liu, H. Bi, D. He, L. Bai, W. Wang, H. Yuan, Q. Song, P. Su, Z. Zang, T. Zhou, J. Chen, *ACS Energy Lett.* **2021**, *6*, 2526–2538.
[22] J. Chen, N. G. Park, *Adv. Mater.* **2019**, *31*, 1803019.
[23] S. You, H. Zeng, Y. Liu, B. Han, M. Li, L. Li, X. Zheng, R. Guo, L. Luo, Z. Li, *Science* **2023**, *379*, 288–294.
[24] Y. Shen, K. Deng, Q. Chen, G. Gao, L. Li, *Adv. Mater.* **2022**, *34*, 2200978.
[25] D. He, D. Ma, R. Li, B. Liu, Q. Zhou, H. Yang, S. Lu, Z. Zhang, C. Li, X. Li, J. Chen, *ACS Energy Lett.* **2024**, *9*, 2615–2625.
[26] Q. Fu, H. Liu, S. Li, T. Zhou, M. Chen, Y. Yang, J. Wang, R. Wang, Y. Chen, Y. Liu, *Angew. Chem.* **2022**, *134*, e202210356.
[27] P. Yan, D. Yang, H. Wang, S. Yang, Z. Ge, *Energy Environ. Sci.* **2022**, *15*, 3630–3669.
[28] Z. Yao, F. Zhang, Y. Guo, H. Wu, L. He, Z. Liu, B. Cai, Y. Guo, C. J. Brett, Y. Li, *J. Am. Chem. Soc.* **2020**, *142*, 17681–17692.
[29] M. H. Li, S. C. Liu, F. Z. Qiu, Z. Y. Zhang, D. J. Xue, J. S. Hu, *Adv. Energy Mater.* **2020**, *10*, 2000501.
[30] J.-Y. Seo, H.-S. Kim, S. Akin, M. Stojanovic, E. Simon, M. Fleischer, A. Hagfeldt, S. M. Zakeeruddin, M. Grätzel, *Energy Environ. Sci.* **2018**, *11*, 2985–2992.
[31] Y. Gao, Z. Song, Q. Fu, Y. Chen, L. Yang, Z. Hu, Y. Chen, Y. Liu, *Adv. Mater.* **2024**, *36*, 2405921.
[32] J. Li, Q. Dong, N. Li, L. Wang, *Adv. Energy Mater.* **2017**, *7*, 1602922.
[33] S. Wu, R. Chen, S. Zhang, B. H. Babu, Y. Yue, H. Zhu, Z. Yang, C. Chen, W. Chen, Y. Huang, *Nat. Commun.* **2019**, *10*, 1161.
[34] E. Bi, W. Tang, H. Chen, Y. Wang, J. Barbaud, T. Wu, W. Kong, P. Tu, H. Zhu, X. Zeng, *Joule* **2019**, *3*, 2748–2760.
[35] J. Xu, P. Shi, K. Zhao, L. Yao, C. Deger, S. Wang, X. Zhang, S. Zhang, Y. Tian, X. Wang, *ACS Energy Lett.* **2024**, *9*, 1073–1081.
[36] J. Tao, J. Xue, H. Guo, Y. Wang, J. Shen, T. Wang, T. He, G. Fu, S. Yang, *Chem. Eng. J.* **2023**, *463*, 142445.
[37] H. Zhang, F. T. Eickemeyer, Z. Zhou, M. Mladenović, F. Jahanbakhshi, L. Merten, A. Hinderhofer, M. A. Hope, O. Ouellette, A. Mishra, *Nat. Commun.* **2021**, *12*, 3383.
[38] X. Wu, Y. Jiang, C. Chen, J. Guo, X. Kong, Y. Feng, S. Wu, X. Gao, X. Lu, Q. Wang, *Adv. Funct. Mater.* **2020**, *30*, 1908613.

[39] T.-S. Su, F. T. Eickemeyer, M. A. Hope, F. Jahanbakhshi, M. Mladenovic, J. Li, Z. Zhou, A. Mishra, J.-H. Yum, D. Ren, *J. Am. Chem. Soc.* **2020**, *142*, 19980–19991.
[40] X. Chen, C. Deng, J. Wu, Q. Chen, Y. Du, Y. Xu, R. Li, L. Tan, Y. Wei, Y. Huang, *Adv. Funct. Mater.* **2024**, *34*, 2311527.
[41] Z. Wan, H. Lu, J. Yang, Y. Zhang, F. Lin, J. Xia, X. Yao, J. Luo, C. Jia, *J. Energy Chem.* **2022**, *74*, 489–496.
[42] R. Chen, Y. Wu, Y. Wang, R. Xu, R. He, Y. Fan, X. Huang, J. Yin, B. Wu, J. Li, *Adv. Funct. Mater.* **2021**, *31*, 2008760.
[43] T. Wang, Y. Zhang, W. Kong, L. Qiao, B. Peng, Z. Shen, Q. Han, H. Chen, Z. Yuan, R. Zheng, *Science* **2022**, *377*, 1227–1232.
[44] J. Y. Seo, S. Akin, M. Zalibera, M. A. R. Preciado, H. S. Kim, S. M. Zakeeruddin, J. V. Milić, M. Grätzel, *Adv. Funct. Mater.* **2021**, *31*, 2102124.
[45] T. Ye, W. Chen, S. Jin, S. Hao, X. Zhang, H. Liu, D. He, *ACS Appl. Mater. Interfaces* **2019**, *11*, 14004–14010.
[46] F. Gao, C. Luo, X. Wang, C. Zhan, Y. Li, Y. Li, Q. Meng, M. Yang, K. Su, D. Yuan, *Adv. Funct. Mater.* **2023**, *33*, 2211900.
[47] T. Chen, X. Li, Y. Wang, F. Lin, R. Liu, W. Zhang, J. Yang, R. Wang, X. Wen, B. Meng, *J. Energy Chem.* **2023**, *79*, 382–389.
[48] P. Lopez-Varo, M. Amara, S. Cacovich, A. Julien, A. Yaiche, M. Jouhari, J. Rousset, P. Schulz, J.-F. Guillemoles, J.-B. Puel, *Sustain. Energy Fuels* **2021**, *5*, 5523–5534.
[49] Q. Zhou, D. He, Q. Zhuang, B. Liu, R. Li, H. Li, Z. Zhang, H. Yang, P. Zhao, Y. He, Z. Zang, J. Chen, *Adv. Funct. Mater.* **2022**, *32*, 2205507.
[50] M. V. Khenkin, E. A. Katz, A. Abate, G. Bardizza, J. J. Berry, C. Brabec, F. Brunetti, V. Bulović, Q. Burlingame, A. Di Carlo, *Nat. Energy* **2020**, *5*, 35–49.

Manuscript received: August 29, 2024
Accepted manuscript online: November 3, 2024
Version of record online: November 16, 2024